Visual Abstract

Effect of nano-clay addition and heat treatment on tensile and stress-controlled low-cycle fatigue behaviors of aluminum-silicon alloy

A. Basiri, A. Dadashi, M. Azadi
Faculty of Mechanical Engineering, Semnan University, Semnan, Iran
m_azadi@semnan.ac.ir, http://orcid.org/ 0000-0001-8686-8705

G. Winter, B. Seisenbacher, F. Grün
Chair of Mechanical Engineering, Montanuniversität Leoben, Leoben, Austria

ABSTRACT. The objective of the present paper is to investigate the stress-controlled low-cycle fatigue behavior of piston aluminum-silicon (AlSi) alloy reinforced with nano-clay particles and T6 heat treatment. The piston aluminum-silicon alloy strengthened by 1 *wt.*% nano-clay particles were prepared by the stir casting method and then subjected to the heat treatment. The optical microscopy analysis demonstrates that the heat treatment changed the size, morphology, and distribution of silicon phases through the microstructure of the aluminum matrix. In addition to tensile tests, stress-controlled low-cycle fatigue experiments at different loading conditions including the variation of the mean stress, the stress rate, and the stress amplitude were conducted at room temperature. The obtained experimental results showed no clear improvement in either mechanical or fatigue properties of the material. Moreover, the density measurements using the Archimedes method reveal a higher content of the porosity in nano-composite. It was observed that the reinforcement (nano-particles and the heat treatment) can change the cyclic behavior of the AlSi alloy, significantly. The cyclic hardening feature of the AlSi alloy changed to cyclic softening and also the fatigue lifetime and the ratcheting resistance decreased after the nano-particles addition and the heat treatment. Through the microstructural analysis, it was indicated that the neglecting of higher kinematics of age hardening in nano-composite was the major source of mechanical properties reduction. In the end, it was shown that the fatigue lifetime of samples can be described adequately utilizing a modified plastic strain energy technique considering the mean stress effect.

KEYWORDS. Aluminum-silicon alloys; Stress-controlled cyclic behavior; Fatigue lifetime; Nano-clay-particles; Heat treatment.

OPEN ACCESS

Citation: Basiri, A., Dadashi, A., Azadi, M., Gruen, F., Winter, G., Seisenbacher, B., Effect of nano-clay addition and heat treatment on tensile and stress-controlled low-cycle fatigue behaviors of aluminum-silicon alloy, Frattura ed Integrità Strutturale, 57 (2021) 373-397.

Received: 21.05.2021
Accepted: 17.06.2021
Published: 01.07.2021

INTRODUCTION

Pistons in internal combustion engines are one of the critical and heavy-duty components, which are subjected to Low-cycle Fatigue (LCF) and wear damages during engine performance [1,2]. Therefore, the utilized material should provide high resistance under cyclic loadings and also high strength to weight ratio for the fuel consumption and consequently reducing the gas emission. For this purpose, the aluminum-silicon alloys are a potential candidate because of their high strength to weight ratio, good castability, acceptable ductility, and corrosion resistance [3]. There are several concepts available that could achieve improvements in mechanical and fatigue properties through the piston design including the optimized geometries, novel materials, advanced manufacturing processes, and different strengthening methods [1]. One of the most common strengthening methods is the development of metal-matrix composites reinforced with ceramic particles, which have attracted great attention over the past decade [4].

Several studies [5-7] had demonstrated the superior mechanical properties of aluminum-matrix nano-composites in comparison to similar micro-composites with the same volume fraction of particles. In the context of the cyclic behavior, LCF properties of particle-reinforced aluminum-matrix composites had been investigated in the literature extensively [8-12]. Results indicate the inferior fatigue lifetime compared to their counterpart monolithic alloys. This was mainly due to the limited ductility of the metal matrix in the presence of the ceramic particles contrary to High-cycle Fatigue (HCF), in which the fatigue lifetime was mostly strength-dependent. Llorca [13] indicated that the particle cracking was the major source of the fatigue crack initiation and growth through the matrix in composites. On the other hand, Wallin et al. [14] pointed out that the particle fracture probability could be decreased by the particle size reduction. Therefore, it was desirable to investigate the LCF behavior of metallic materials reinforced by nano-sized ceramic particulates. Senthilkumar et al. [15] conducted fully reversed LCF tests on two materials including AA2014 aluminum alloy containing micro- and nano-Al_2O_3 particles and its counterpart micro-composite, which were both followed by hot extrusion and T6 heat treatment. They showed that the hybrid micro/nano-composite offered a higher fatigue lifetime and cyclic hardening at high strain amplitudes in comparison to almost stabilized response of the micro-composite. Azadi et al. [16] conducted fully-reversed strain-controlled LCF experiments on piston aluminum alloys and their counterpart nano-clay reinforced and T6 heat-treated nano-composites at different temperatures. They concluded that the fatigue behavior of the aluminum alloys was not influenced significantly by nano-particles and the heat treatment except a lifetime reduction at the temperature of 300 $^{\circ}C$ due to the over-aging phenomenon. Ghasemi Yazdabadi et al. [17] studied HCF and LCF responses of an aluminum alloy reinforced with nano-SiC particulates prepared by the powder metallurgy route. They showed that the HCF resistance of nanocomposites improved followed by increasing the tensile strength while increasing the volume fraction. However, the LCF lifetime reduced as a result of the limited slip distance of dislocations caused by hard particles. Jabbari et al. [18] conducted strain-controlled LCF experiments on extruded AZ31B magnesium alloy reinforced by nano-Al_2O_3 particles at different temperatures. They indicated that although the mechanical properties of the material degraded at elevated temperatures, the fatigue lifetime increased as a result of ductility enhancement. Besides, they showed that the Jahed-Varvani model was able to describe the fatigue lifetime of the material appropriately.

The common feature of aforementioned LCF tests is that they have been conducted under strain-controlled conditions. However, it is difficult to realize the cyclic loading mode in the actual service condition of the components since strains and stresses are related to each other by some constitutive behaviors. Therefore, knowing both the strain and stress fields and the relation between them in a component would allow both stress- and strain-controlled tests to be used to identify the fatigue behavior of the materials [19,20]. An important field of this area is stress-controlled LCF accompanying mean stress, which usually results in ratcheting i.e., the progressive accumulation of the inelastic strain and consequently to premature fatigue failure. The investigation of symmetric and asymmetric stress-controlled LCF behavior of aluminum alloys had been performed during recent years in the literature [21-26] but not as extensively as steel and magnesium alloys. In the context of the stress-controlled LCF experiments on metal-matrix composites, the ratcheting deformation in 6061 aluminum alloy reinforced with SiC particulates was systematically discussed by Kang [27] and Kang and Liu [28]. The effects of the particulate volume fraction, the heat treatment, the multiaxiality, the temperature, and some other factors on the ratcheting were discussed. Useful results along their purposes were that the ratcheting resistance of composite increased as the SiC volume fraction enhanced. Besides, the ratcheting behavior of composite had a great time-dependence even at low temperatures, which implied the presence of the creep component in the total ratcheting deformation. Regarding the stress-controlled LCF loading on nano-composites, Goh et al. [29] investigated the effect of nano-sized Y_2O_3 particulates addition into magnesium alloys in different volume fractions on the cyclic plastic response under stress-controlled LCF loading. They showed that the intensity of cyclic hardening in nano-composite increased with the volume fraction of reinforcements, which was a result of the forest dislocation's pinning role of dispersed nanoparticles.

Through the above literature review, studies demonstrated the advantage of nano-particles addition [5-7,15-18] and the heat treatment [15,16] on mechanical and fatigue properties improvement of metallic materials. Regardless of the little investigations that were carried out on the strain-controlled LCF behavior of nano-composites [15-18], there was only one investigation [29] focusing on stress-controlled LCF behavior of metal matrix nano-composites to the author's best knowledge. The promising results of such loading conditions in micro-composites [27-28] and also fewer studies on stress-controlled LCF behavior of aluminum alloys [21-26] in comparison to other metallic materials, motivated the present investigation to be made. Therefore, the objective of this article was to evaluate the effect of the addition of nano-clay particles and the heat treatment on mechanical and stress-controlled LCF properties of piston AlSi alloys.

EXPERIMENTAL PROCEDURE

Materials Processing

The matrix material, which was utilized in the present research, was a cast aluminum-silicon (AlSi) alloy (ENAC-48000). This AlSi12CuNiMg alloy had been widely utilized in the manufacturing of engine pistons in automotive industries. In the primary ingots of this AlSi alloy, the chemical composition is measured as Si: 12.7 *wt.%*, Ni: 0.8 *wt.%*, Cu: 1.16 *wt.%*, Fe: 0.56 *wt.%*, Mg: 1.00 *wt.%*, Zn: 0.16 *wt.%*, Mn: 0.12 *wt.%* and the aluminum as balance. Two groups of specimens were made in this research, including aluminum alloy specimens reinforced with nano-clay particles and the original un-reinforced alloys for comparison. The fabrication method of original aluminum alloys is a permanent mold gravity casting method described in the following paragraph:

The aluminum ingots were first melted and the temperature was held at 700 °*C* for 2 hours in an electrical resistance furnace [30,31] before pouring them into a permanent steel mold. For the production of 1 *wt.%*, nano-clay particles reinforced specimens with the stir-casting process, clay (type: montmorillonite K10) as nano-particles with the chemical composition according to Tab. 1 were used. In this research, nano-clay particles were first pre-heated to the temperature of 420 °*C* for 20 minutes [31,32] to achieve a better wettability of nano-clay particles in the aluminum melt. The nano-particles powder was wrapped in aluminum foil. Then, they were added gradually to the aluminum melt. The clay amount is 2 g by 2 g in order to eliminate any gas accumulations in the aluminum melt. The density of the nano-clay particles (0.5 g/cm^3) was lower than that of the molten aluminum. The density of the aluminum alloy was 2.7 g/cm^3. This causes the floating of nano-particles in the crucible surface. To get an appropriate distribution of reinforcements in a uniform condition in the molten aluminum alloy, a steel stirrer was used. This stirrer was redesigned in order to have a falling stream in the melt through the casting process. It should be noted that high stirring time and rotational speed can result in better dispersion of nano-particles in the melt. On the other hand, it caused the degradation of mechanical properties because of the formation of some undesired chemical components and increasing the gas entrapment in the melt [6,30,33]. It should be noted that for the nano-composite, it took 20 minutes to put the molten aluminum in the steady-state condition after adding the nano-clay particles. Then, the resulting composite slurry was poured into the cast-iron mold.

	Oxides (%)								
Material	SiO_2	Al_2O_3	TiO_2	Fe_2O_3	MgO	CaO	K_2O	Na_2O	LOI
Nano-clay	50.95	19.60	0.62	5.62	3.29	1.97	0.86	0.98	15.45

Table 1: The chemical composition of nano-clay particles.

After the casting process, all initial cylinders of aluminum alloys and nano-composites were cooled down in the air. Then, the machining process was performed to fabricate the standard-sized samples from initial casted cylinders. For these specimens, the geometry, which is suited for both tensile and fatigue tests, is illustrated in Fig. 1. In addition, mechanical polishing was done to have a mirror-like surface.

After machining, the nano-composite specimens were subjected to T6 heat treatment to the following schedule: a solution treatment of the alloy at 500 °*C* for 1 hour, water quenching and then artificial aging at 300 °*C* for 2 hours (air-cooled) [16,34].

Microstructural Evaluation

For investigating the material microstructure, aluminum alloy and nano-composite specimens were firstly mounted. This job was done with the Struers Citopress embedding device. Then, they were subjected to a five-step grinding process at 300

rpm and under 4 *N*. Moreover, the last stage for having smooth surfaces was four-step polishing in the water-based diamond lubricant and also was using the etchant of Keller's reagent solution. Microstructural characterizations before testing were carried out using the optical microscopy (OM) of Keyence VHX5000. In addition, the ICNA energy dry cool 350 was utilized as the energy-dispersive X-ray spectroscopy (EDS). For the image of the field emission scanning electron microscopy (FE-SEM), the JEOL-7200F equipment was also used. Furthermore, the porosity content of the samples as a measure of void spaces in the materials was determined by comparing the measured density of the samples using the Archimedes method with that of their theoretical density. The details of this method were referred to in the literature [35].

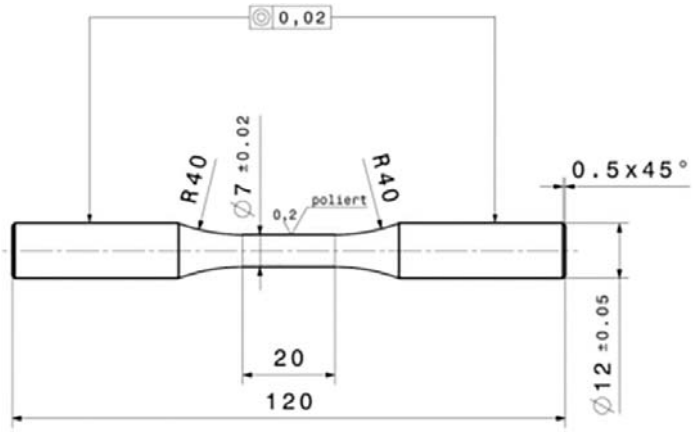

Figure 1: The geometry for samples used in tensile and fatigue tests (dimensions in mm).

Tensile and Fatigue Testing

Uniaxial tensile and LCF experiments were carried out using an automated mechanical testing machine (Instron Servo-hydraulic testing machine), equipped with the 100 *kN* load cell. Instron room temperature extensometer was used in order to measure the strain value through the test. Tensile tests were done at a constant strain rate of 2.5×10^{-3} s^{-1} at room temperature, based on the ASTM E8M standard testing procedure [36].

The fatigue tests were carried out in a tension-compression engineering stress-controlled loading mode at room temperature according to the standard fatigue testing procedure of ASTM E466 [37]. The response of materials to varied the stress amplitude, the mean stress and the stress rate were examined and the detailed loading conditions for original aluminum alloys and nano-composites are presented in Tabs. 2 and 3, respectively. It should be noted that σ_a was the stress amplitude, σ_m was the mean stress and $\dot{\sigma}$ was the stress rate.

Since the cyclic loading condition was tensile-compressive, the stress distribution was uniform on the cross section of the sample. Therefore, cracks would initiate either on the specimen surface (through the gauge length) or inside the sample. However, the fatigue lifetime of samples was defined as the cycle number, corresponding to the first abrupt reduction of the load carrying capacity in the strain amplitude diagram versus the number of cycles. It should be noted that "AlSi" was used for the original aluminum alloy (without reinforcement) and "AlSi_N_T6" referred to the heat-treated nano-composite through the rest of the paper.

Sample No.	σ_a (*MPa*)	σ_m (*MPa*)	$\dot{\sigma}$ (*MPa/s*)
3	200	0	100
6	200	10	100
4	200	20	100
9	210	0	10
11	210	0	100
10	210	0	1000
8	220	0	10
7	220	0	100
5	220	0	1000

Table 2: Loading conditions in stress-controlled fatigue tests on AlSi.

Sample No.	σ_a (MPa)	σ_m (MPa)	$\dot{\sigma}$ (MPa/s)
13	200	0	10
8	200	0	100
12	200	0	100
4	200	10	100
3	200	20	100
14	200	0	1000
10	210	0	10
9	210	0	100
5	210	0	1000
2	220	0	100
11	190	0	100

Table 3: Loading conditions in stress-controlled fatigue tests on AlSi_N_T6.

RESULTS AND DISCUSSION

Microstructure Characterization

The optical micrographs of original aluminum alloys (AlSi) and heat-treated nano-composites (AlSi_N_T6) were depicted in Fig. 2-5. As a first observation, the finer microstructure of AlSi_N_T6 compared to AlSi alloys could be observed. It was commonly confirmed that the addition of hard particles to the metal-matrix materials resulted in reduction of the grain size [5,30], which was generally related to the pinning role of particles at the grain boundaries during the solidification. Such a phenomenon in the nano-composites can improve the mechanical strength of the matrix material through the Hall-Petch effect [38].

Considering Figs. 4 and 5, in the microstructure of AlSi alloys, four different phases could be distinguished. The first phase was the aluminum (α-Al) matrix with the white color. The second one is the AlSi phase with the dendritic morphology that is homogeneously distributed in the matrix. The third one is the silicon (Si) phase as a gray-colored area and finally, intermetallic phases as black-colored and light gray-colored script-like areas. Similar phases could be found in AlSi_N_T6, but a change in the shape and also the distribution of both Si phases and intermetallic phases could be observed as a result of the nano-particles addition and the heat treatment. In the following paragraphs, a discussion on the size and morphology of both Si and intermetallic phases, which can determine the mechanical and fatigue behavior of the material has been performed.

As could be observed qualitatively in Fig. 5, the content of the Si phase was increased for AlSi_N_T6 compared to AlSi alloys. This could be a result of the presence of about 50% SiO_2 in the chemical composition of nano-clay particles according to Tab. 1. As reported in the literature [39], the Si phase in the piston aluminum alloys was usually detected to exist in two types including the flake shape and the coarse primary blocky shape, in which the primary Si phase had a dominant role in the determination of mechanical properties [40-41]. Based on reports in the previous research [16], the circularity of the Si phase increased as a result of the heat treatment that implied a higher number of blocky shape Si particles compared to the needle shape ones in AlSi_N_T6. This result was consistent with the reports in the literature [42-44], which states that after the heat treatment, Si particles tend to become spherical. Such results can cause an improvement in the mechanical properties [40,44]. Besides, the size of blocky Si particles increased as a result of nano-particles and the heat treatment, which could be a source of reduction in fatigue lifetime and mechanical properties in the base metal [43].

The distribution of intermetallic phases was similar in both AlSi alloy and also AlSi_N_T6. However, it was demonstrated quantitatively in the previous research [16] that the content of these phases and their sizes in AlSi-N_T6 were lower than the base AlSi alloys. Lower content and size of intermetallic phases were reported to cause better fatigue performance [45-46].

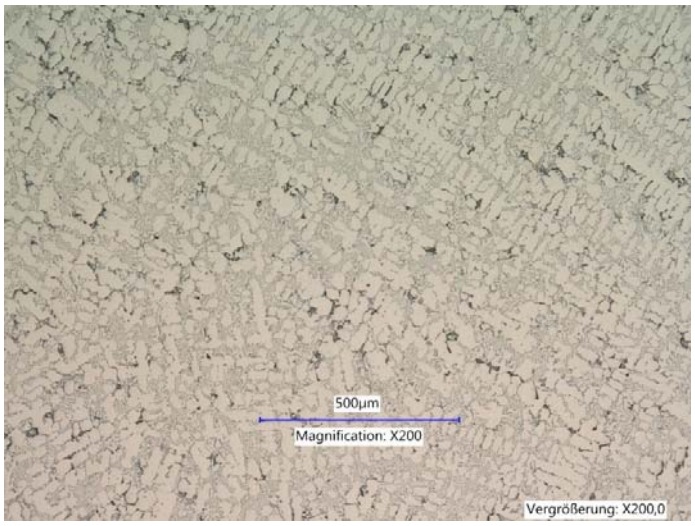

Figure 2: Optical micrograph images of AlSi samples with 200X magnification.

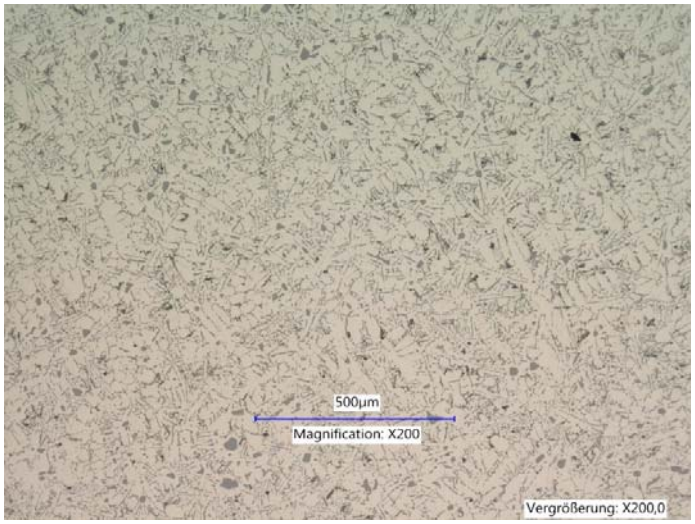

Figure 3: Optical micrograph images of AlSi_N_T6 samples with 200X magnification.

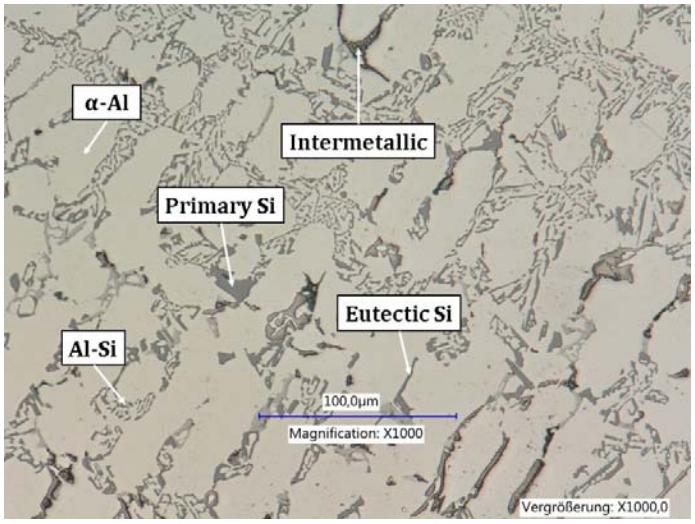

Figure 4: Optical micrograph images of AlSi samples with 1000X magnification.

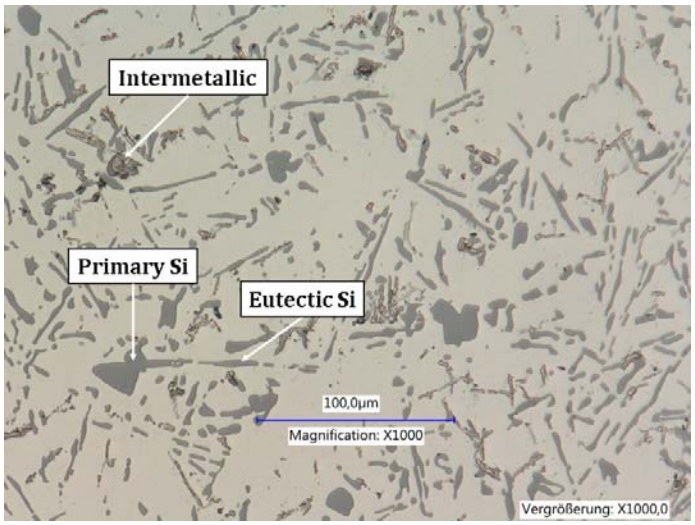

Figure 5: Optical micrograph images of AlSi_N_T6 samples with 1000X magnification.

To study the material microstructures more accurately, the FE-SEM images were depicted in Fig. 6-7 for both AlSi alloys and AlSi_N_T6. The Intermetallic phases could be distinguished easily from the rest of the microstructure. As it could be observed, the intermetallic phases in AlSi_N_T6 have a nearly needle-shaped morphology, which could act as stress-concentration sites and eventually reduce mechanical properties [47]. For the determination of the dominant chemical element of intermetallic phases, the EDS results for AlSi_N_T6 were depicted in Fig. 8. Both Si and intermetallic phases could be found through the aluminum matrix. The elements, which have percentages of more than 1% including Al, Si, Cu, Mg, and O according to Tab. 1, were presented. As it could be observed, two main intermetallic phases including Cu-rich and Mg-rich could be distinguished. The presence of such intermetallic phases could result in the improvement of mechanical properties [48].

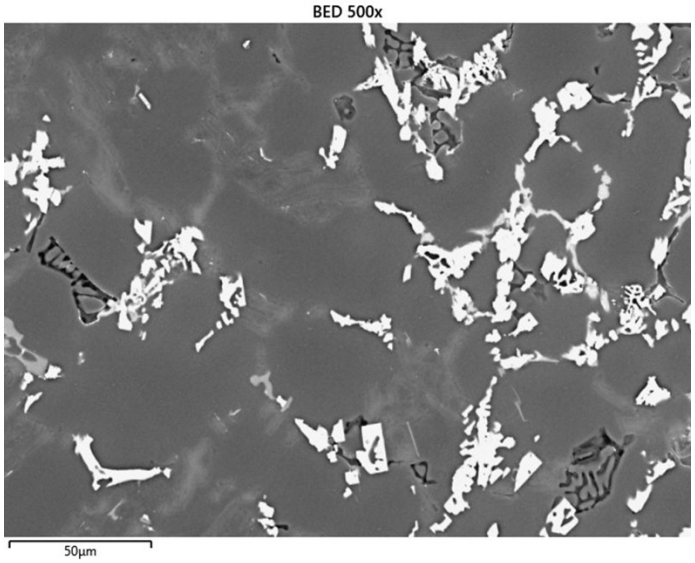

Figure 6: FE-SEM images of AlSi with low magnifications.

It is widely accepted that nano-particles have a high tendency to attract each other and create agglomerations as a result of their high surface to volume ratio. The agglomerations are a possible site for the crack nucleation and therefore, could be the reason for achieving undesirable mechanical properties compared to the original metal matrix. Nevertheless, reaching completely distributed single nano-particles is quite impossible in most cases [7]. The dispersion of nano-particles in the metal matrix is highly dependent on the processing route. Fig. 9-10 demonstrates the FE-SEM images of the surface of

AlSi_N_T6 sample at two typical sites. Fig. 9 exhibits the nano-clay particle distribution in the aluminum matrix. A highly magnified FE-SEM image for AlSi_N_T6 at a clustered particle site is depicted in Fig. 10 and its counterpart EDS results in Fig. 11. The elements, which had percentages more than 1% including Al, Si, Cu, Mg, and O according to Tab. 1, were presented. From Fig. 11, it was easy to recognize the nano-particles dispersed in the aluminum matrix by focusing on the two most abundant elements including Si and O in the nano-clay chemical composition. Observations indicated that the dispersion of nano-particles was proper but not perfect and so desirable and therefore, some small degrees of agglomerations were detected in the microstructure.

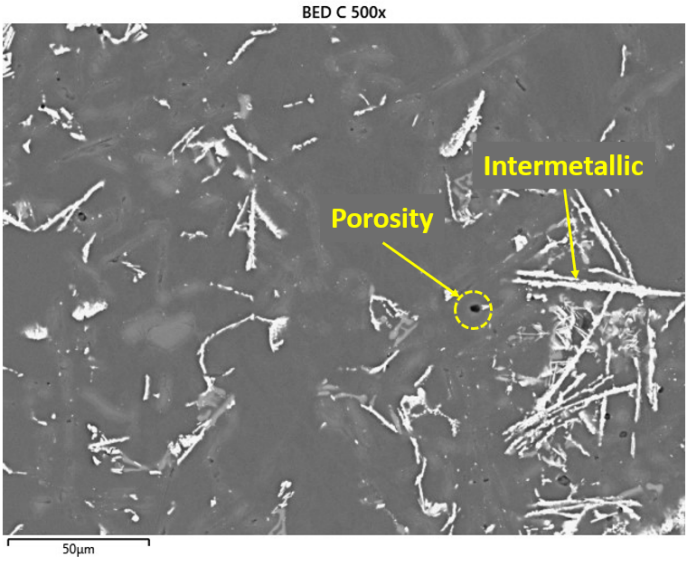

Figure 7: FE-SEM images of AlSi_N_T6 with low magnifications.

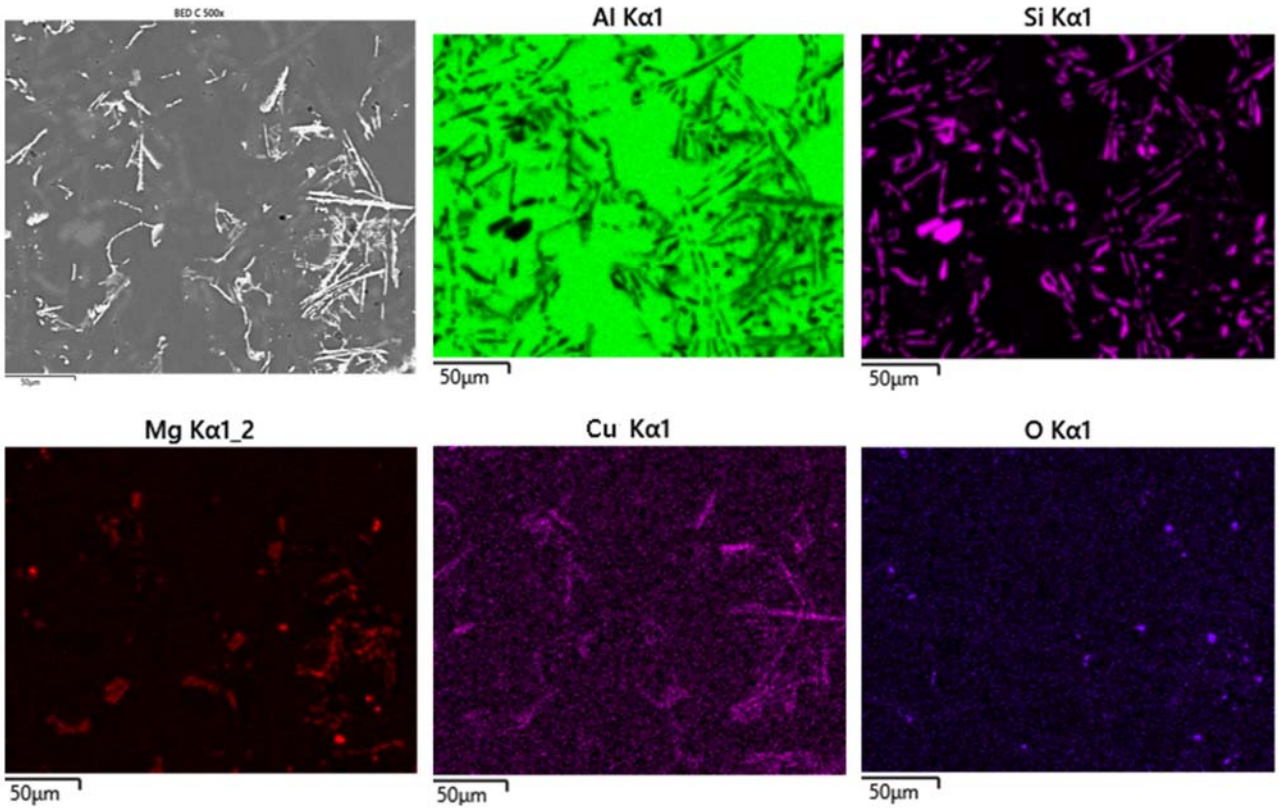

Figure 8: EDS results for AlSi_N_T6 with low magnifications [16].

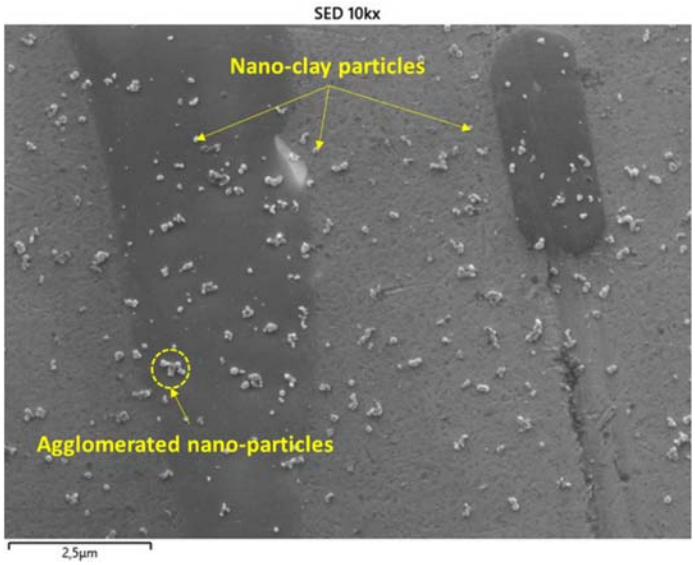

Figure 9: FE-SEM images of AlSi_N_T6 sample at a region of dispersed particles.

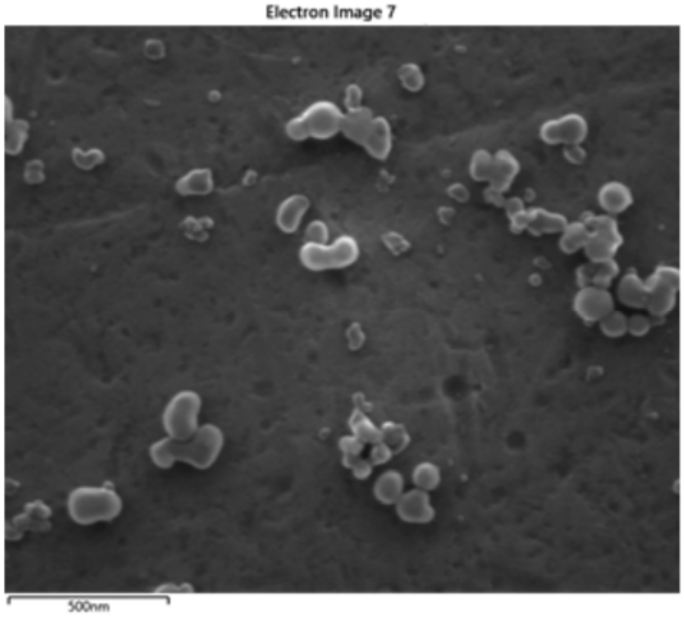

Figure 10: FE-SEM images of AlSi_N_T6 sample at highly clustered particles region.

Density Measurement

It could be observed in Fig. 7 that some black tiny areas were present in the microstructure of AlSi_N_T6, which represents the micro-porosity areas. It has been indicated in several studies [7,49-50] that an enhancement in micro-porosity content would be achieved after nano-particles addition to the metal matrix, which results in mechanical properties degradation. Such a phenomenon was mainly attributed to poor wettability features of ceramic particulates [7,49], which stimulated the pore nucleation at nano-particles sites or agglomeration sites.

The results of the pore measurement of both AlSi and AlSi_N_T6 using the Archimedes method are presented in Tab. 4. As it could be seen in Tab. 4, the porosity content of AlSi_N_T6 has increased in comparison to its counterpart AlSi alloy following the reports in the literature [7,49-50].

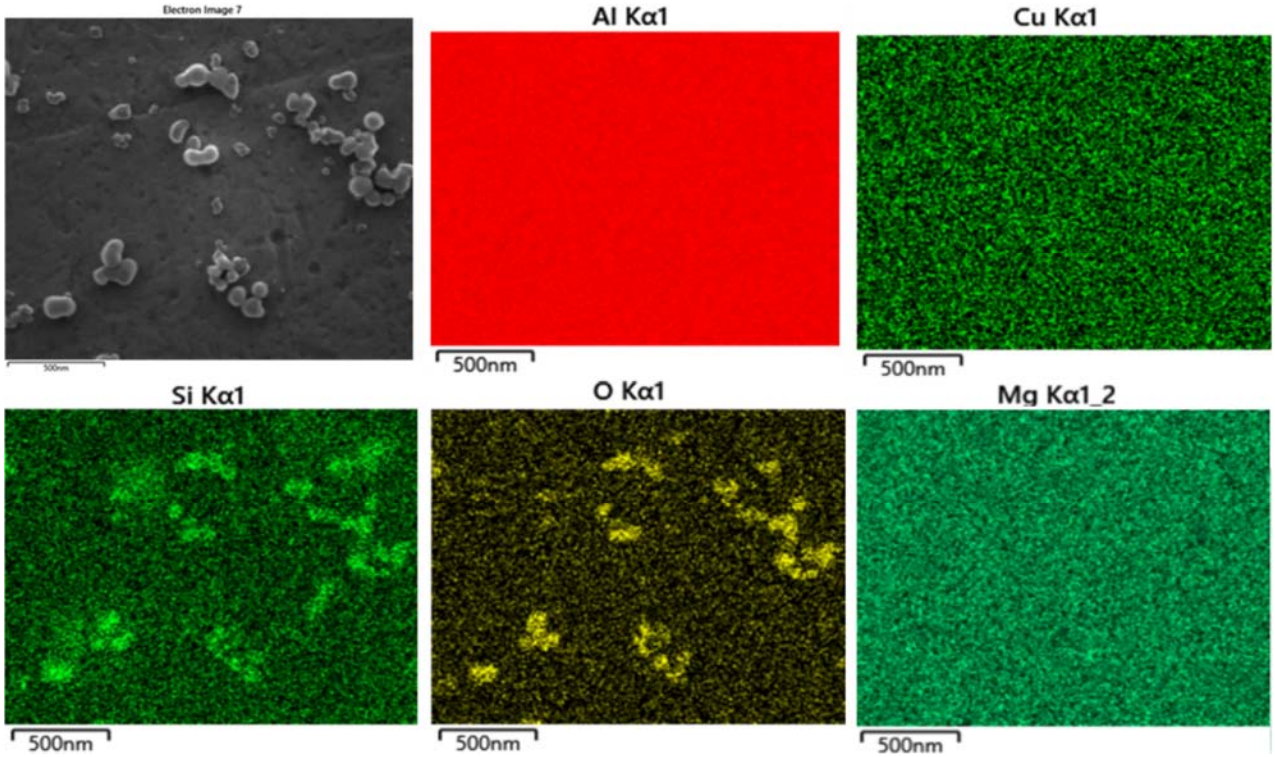

Figure 11: EDS results with high magnifications for AlSi-N_T6.

	Measured density (g/cm^3)	Theoretical density (g/cm^3)	Porosity (%)
AlSi	2.6813	2.7000	0.67
AlSi_N_T6	2.6571	2.5862	2.74

Table 4: Results of the pore measurement.

Tensile Properties

The tensile flow curves of AlSi alloys and AlSi_N_T6 are depicted in Fig. 12. Moreover, the measured mechanical properties corresponding to tensile curves were presented in Tab. 5. Based on the results, AlSi_N_T6 showed different tensile properties compared to AlSi alloys. The yield strength and also the ultimate tensile strength in the nano-composite reduced by 7% and 5% respectively. In addition, the elastic modulus decreased by 21%. However, the elongation percent increased by about 2.5 times with respect to AlSi alloy.

Cyclic behaviors

The results of cyclic deformation had been presented focusing on mean stress, stress amplitude, and stress rate effects, respectively. Fig. 13-16 depicts the first and mid-life hysteresis cycle of both AlSi and AlSi_N_T6 under the stress amplitude of 200 *MPa*, stress rate of 100 *MPa/s*, and different mean stresses. Besides, Fig. 16 demonstrates the evolution of plastic strain amplitude of the mentioned experiments. It could be readily seen in Figs. 13, 14, and 15 the softer response of AlSi_N_T6 in comparison to AlSi alloys. The plastic strain amplitude could be measured as the width of the hysteresis loop, where the horizontal axis is located at the mean stress axis. The softer response of AlSi_N_T6 means a higher plastic strain amplitude and as a consequence a wider hysteresis loop. Besides, the width of hysteresis loops of AlSi alloys demonstrated a decreasing trend, which implies the cyclic hardening behavior, whereas the mentioned width has an increasing trend in AlSi_N_T6, which indicates the cyclic softening behavior of the material. Such an observation had been approved by the evolution of plastic strain amplitude of samples in Fig. 16. It could be seen in Fig. 16 that the AlSi alloys experience a decreasing trend of plastic strain amplitude over cycles, which implies the cyclic hardening feature of piston aluminum alloys. However, the cyclic hardening feature of monolithic alloys had been changed to a cyclic softening feature after the nano-

particles addition and the heat treatment. Besides, as it was reported in the literature [22,23], a higher value of mean stress has resulted in higher responded plastic strain amplitude and also a higher rate of cyclic hardening in the case of AlSi alloys and a higher rate of cyclic softening in the case of AlSi_N_T6.

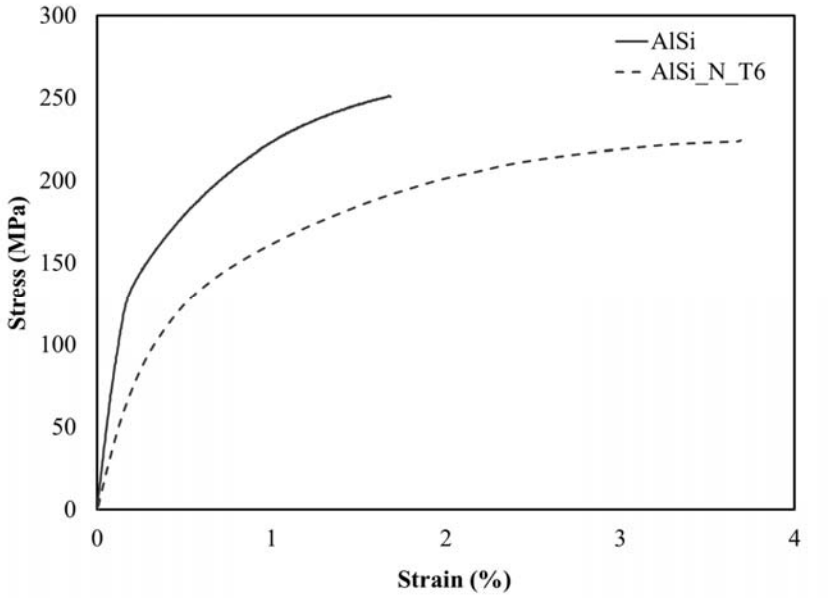

Figure 12: Tensile flow curves of AlSi and AlSi_N_T6.

	AlSi	AlSi_N_T6
Elastic modulus (*GPa*)	85.55±6.26	70.53±7.60
Yield stress (*MPa*)	105.93±10.03	99.12±6.96
Ultimate stress (*MPa*)	236.67±16.21	224.40±10.20
Elongation (%)	1.51±0.23	3.69±0.21

Table 5: Mechanical properties of AlSi and AlSi_N_T6.

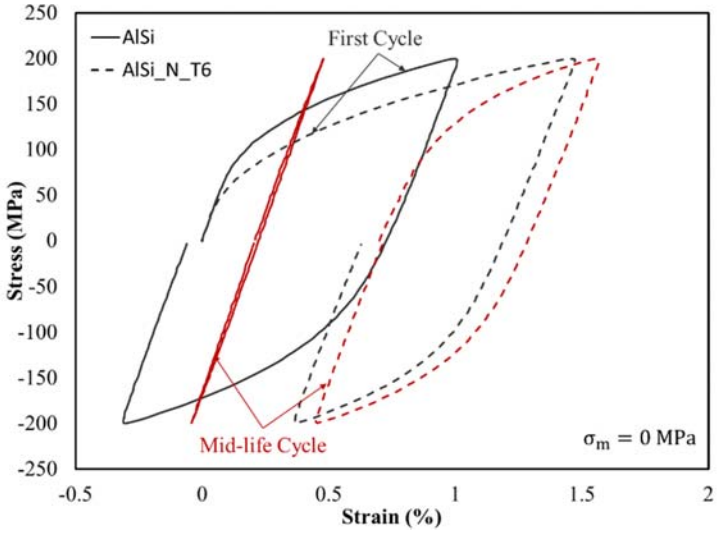

Figure 13: First and mid-life hysteresis loops of AlSi and AlSi_N_T6 under the stress amplitude of 200 *MPa*, the stress rate of 100 *MPa/s* and the mean stress of 0 *MPa*.

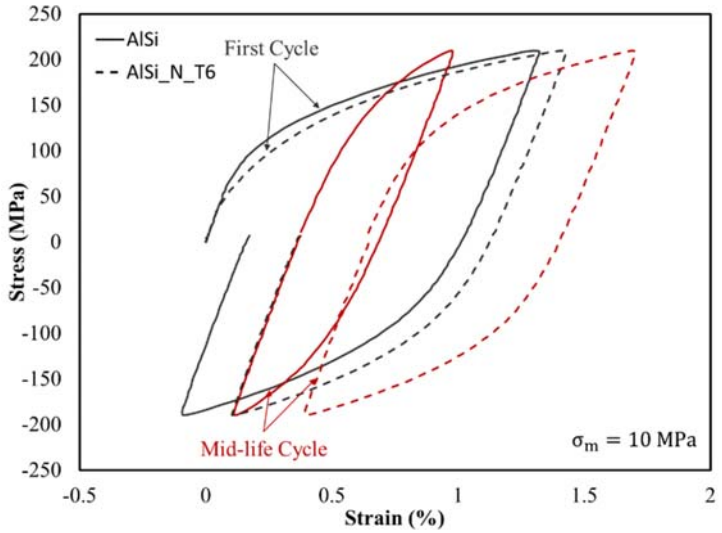

Figure 14: First and mid-life hysteresis loops of AlSi and AlSi_N_T6 under the stress amplitude of 200 *MPa*, the stress rate of 100 *MPa/s* and the mean stress of 10 *MPa*.

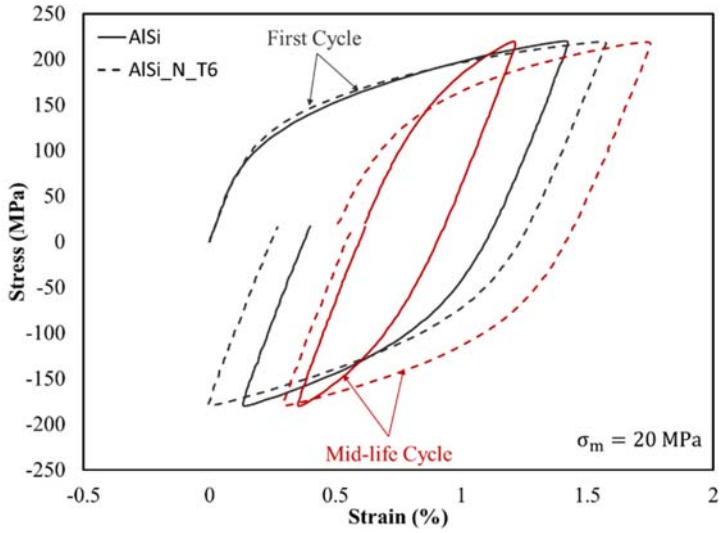

Figure 15: First and mid-life hysteresis loops of AlSi and AlSi_N_T6 under the stress amplitude of 200 *MPa*, the stress rate of 100 *MPa/s* and the mean stress of 20 *MPa*.

In addition to the cyclic softening feature of nano-composites, from Figs. 13, 14, and 15 it is easy to identify the movement of hysteresis loops in the strain axis direction for AlSi_N_T6, which implies the ratcheting deformation. For a better interpretation, the evolutions of strain amplitude and mean strain of both AlSi and AlSi_N_T6 over cycles for the same test conditions in Figs. 13-16 are presented in Figs. 17-18. Fig. 17 indicates another evidence of the cyclic hardening/softening feature of the samples. As it could be observed in Fig. 18, AlSi alloys demonstrated a nearly constant mean strain over cycles, which increased as the mean stress increased. However, after the nano-particles addition and the heat treatment, the mean strain demonstrated an ascending order over cycles, which implies the ratcheting deformation. The rate of ratcheting strain (mean strain), increased as the applied mean stress increased. It is shown in the introduction that cyclic stress loadings with non-zero mean stresses could result in the ratcheting response. Nevertheless, the ratcheting strain for AlSi alloys showed no significant trend counting for the ratcheting behavior even though the applied mean stress for two tests was positive. On the other hand, the applied mean stress in Fig. 13 was zero but still, the ratcheting deformation could be observed in AlSi_N_T6.

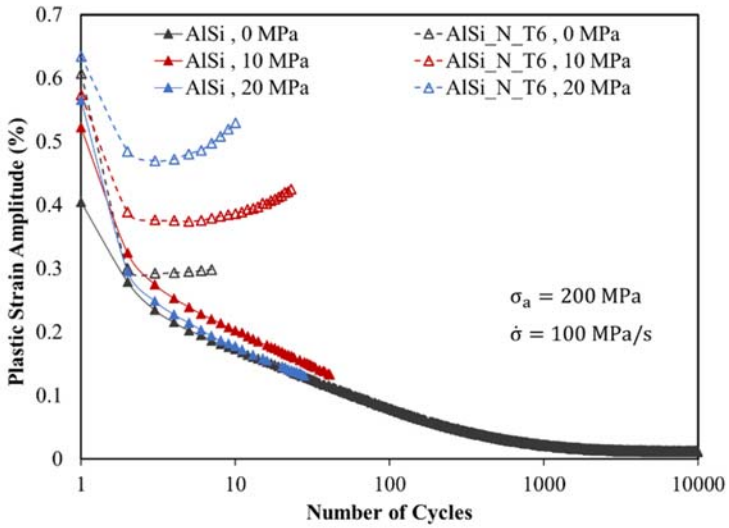

Figure 16: Evolution of plastic strain amplitude of AlSi and AlSi_N_T6 at different mean stresses.

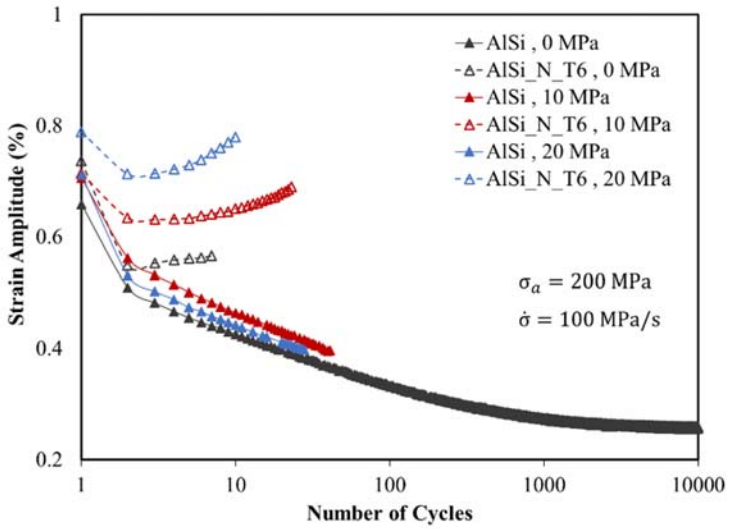

Figure 17: Evolutions of the strain amplitude during cycles under the stress amplitude of 200 *MPa* and the stress rate of 100 *MPa/s*.

Figs. 19-22 depict the test results regarding the stress amplitude effect. In the mentioned tests, the mean stress was equal to zero and the stress rate had been set to 100 *MPa/s*. As commonly noted in the literature [22,23], with increasing the stress amplitude, the strain amplitude also increased and exhibited a higher degree of hardening in the case of the AlSi alloy and softening in the case of AlSi_N_T6. From Fig. 19, a great difference between the response of as-cast AlSi alloys and AlSi_N_T6 to stress amplitude variations could be observed. First of all, despite the zero applied mean stress on these tests, the mean strains were non-zero. This fact could be also confirmed from the curves of the mean strain versus cycles in Fig. 22. Generally, the asymmetrical behavior of the material under fully-reversed cyclic loadings was related to the different deformation mechanisms operating in tension and compression. The tests related to AlSi alloys in Fig. 22 illustrated the tensile mean strain, which implied the larger deformation resistance of the material under tension than compression. However, a nearly constant mean stress sustained most of the fatigue lifetime. This positive mean strain increased as the stress amplitude increased. That was in an agreement with the results in the literature [18,19]. The addition of nano-particles and the heat treatment changed the mean strain response of the material completely. The responded mean strain in AlSi_N_T6 was non-zero under fully-reversed stress-controlled loading similar to AlSi alloys, but with increasing the stress amplitude, the mean strain continuously decreased. It seems that the resistance of the material to the tensile deformation decreased with increasing the stress amplitude and as a consequence, the mean strain changed the polarity from tensile to

compression. It could be observed in Figs. 19 and 22 that under the stress amplitude of 220 *MPa*, the mean strain was completely compressive. Besides, the mean strain was not constant during cycles and despite zero applied mean stress, a ratcheting deformation in tests with stress amplitudes of 200 and 220 *MPa* had been observed.

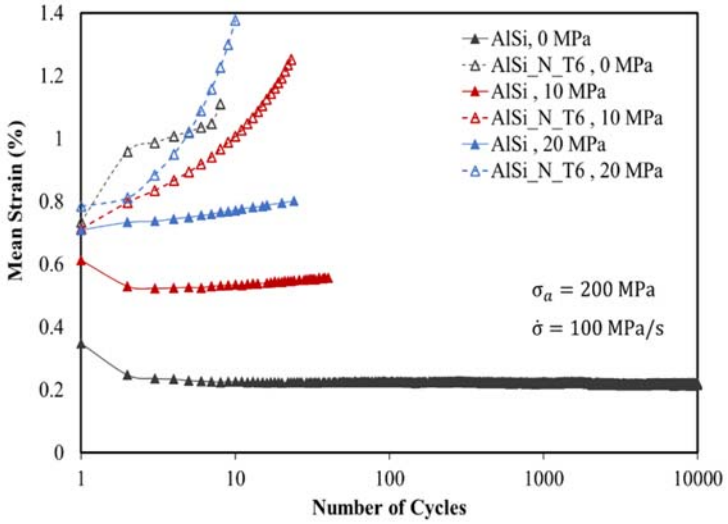

Figure 18: Evolutions of the mean strain during cycles under the stress amplitude of 200 *MPa* and the stress rate of 100 *MPa/s*.

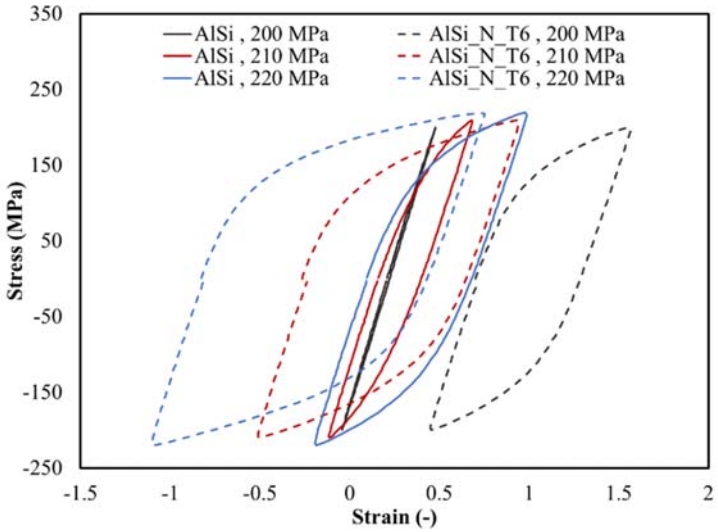

Figure 19: Test results regarding the stress amplitude effect under zero mean stress and the stress rate of 100 *MPa/s* for mid-life hysteresis loops for both AlSi and AlSi_N_T6.

Figs. 23-26 depict the test results regarding the stress rate effect. In the mentioned tests, the mean stress was equal to zero and stress amplitude had been set to 210 *MPa*. It should be noted that experimental data for 10 *MPa/s* of the stress rate on AlSi_N_T6 were eliminated from these figures, due to have only two cycles of loading for the sample.
From Figs. 24 and 25, it could be claimed that both the AlSi alloys and AlSi_N_T6 nano-composites presented a rate-dependent response. The viscosity effect or the time-dependent response normally occurred at high temperatures as a consequence of the creep phenomenon, but it was shown that some materials experienced the viscosity effect even at room temperature. In such materials, the variation in the stress rate influenced the cyclic response [27]. Besides, the sensitivity of nano-composites to the stress rate variations was larger than their counterpart AlSi alloys. Increasing the stress rate, the strain amplitude of AlSi alloys changed negligibly contrary to AlSi_N_T6, which the change of the strain amplitude was significant. The common feature observed in the literature [24-25,51-53], was that with increasing the stress rate, the ratcheting strain decreases in rate-dependent alloys. Considering Figs. 23 and 26, with increasing the loading rate, mean

strain increases in the case of AlSi alloys but after nano-particles and the heat treatment, the mean strain tends to move toward the compressive region as the loading rate increases.
Based on Figs. 24-26 and the tensile test results in Tab. 5, a verification of obtained experimental data could be reported. Since the fatigue lifetime was only some cycles (less than 10 cycles) under high stress levels, near the ultimate strength of studied materials. However, one important note is to have different material behaviors under different stress rates. In other words, tensile testing was done at a different loading rate, compared to the loading rate in LCF testing. Therefore, the results of tensile and fatigue testing could not exactly compare to each other.

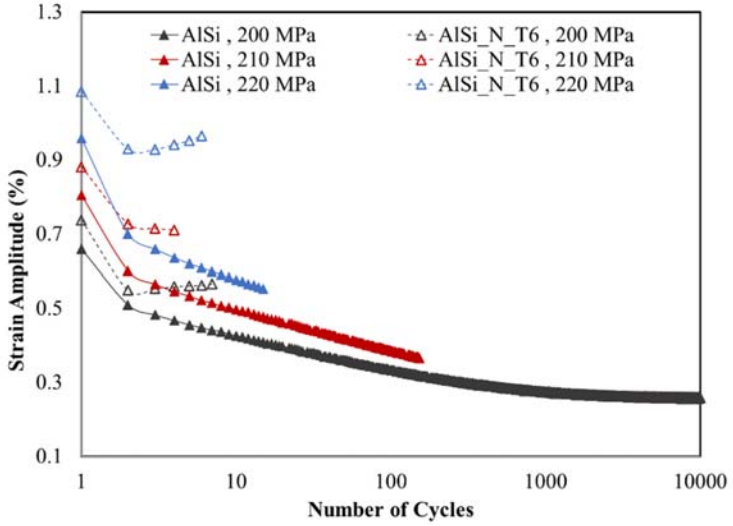

Figure 20: Test results regarding the stress amplitude effect under zero mean stress and the stress rate of 100 *MPa/s* for evolutions of the strain amplitude over cycles for both AlSi and AlSi_N_T6.

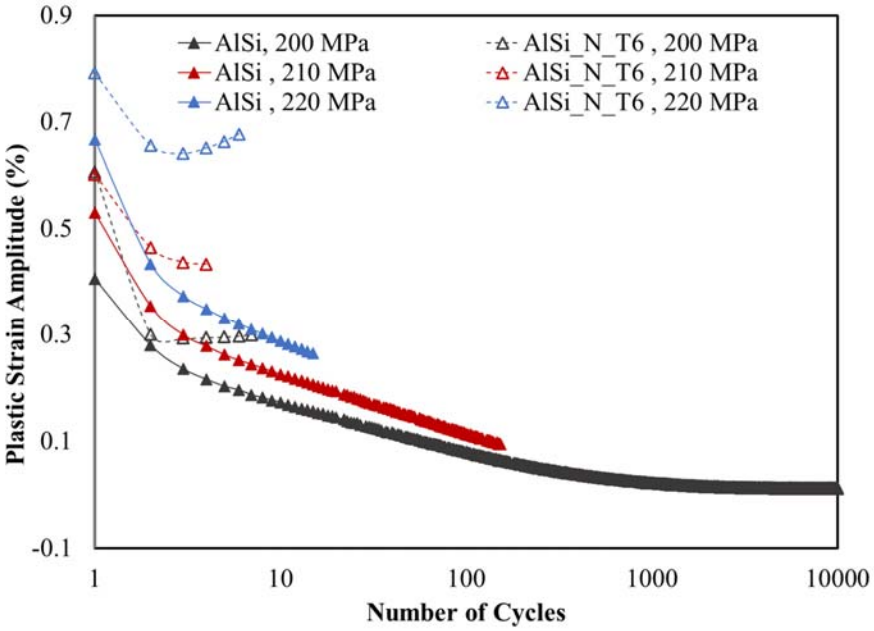

Figure 21: Test results regarding the stress amplitude effect under zero mean stress and the stress rate of 100 *MPa/s* for evolutions of the plastic strain amplitude over cycles for both AlSi and AlSi_N_T6.

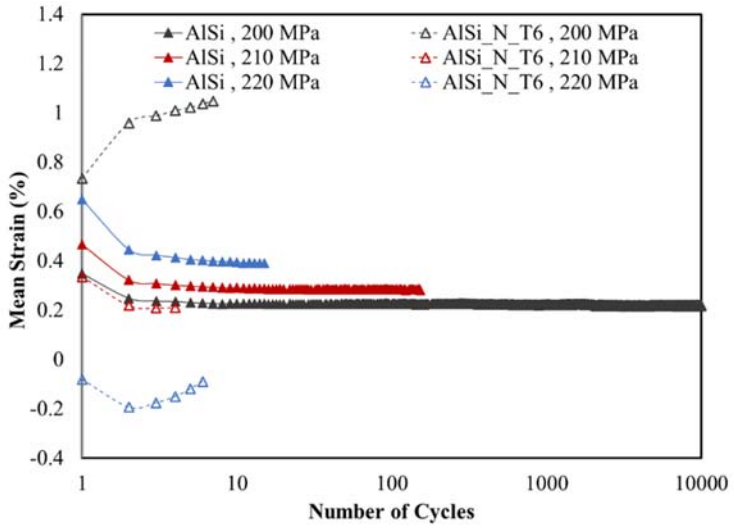

Figure 22: Test results regarding the stress amplitude effect under zero mean stress and the stress rate of 100 *MPa/s* for evolutions of the mean strain over cycles for both AlSi and AlSi_N_T6.

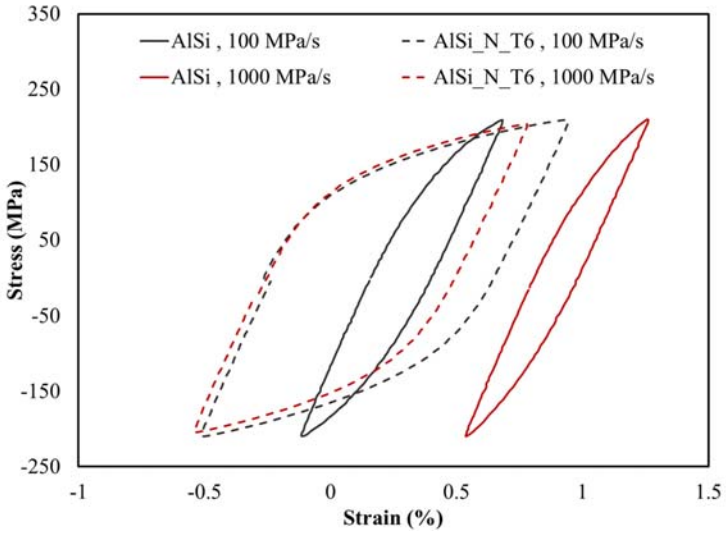

Figure 23: Test results regarding the stress rate effect under zero mean stress and the stress amplitude of 210 *MPa* for mid-life hysteresis loops for both AlSi and AlSi_N_T6.

Fatigue Lifetime prediction

The fatigue life of the samples has been investigated through this sub-section. Generally, in the LCF regime, the strain-based models have been utilized to predict the fatigue lifetime but in the special case of stress-controlled LCF loading, the validity of these models is questionable because of unusual changes in maximum and mean strains during stress-controlled fatigue tests. Therefore, the stress-based models were utilized to predict the fatigue lifetime. Such models [54-55] are presented originally for the high-cycle fatigue (HCF) regime, but some investigations [56-57] demonstrated the validity of these models for the LCF applications.

The classical models like stress- and strain-based models were limited by a constant condition during the fatigue loading, for example, the constant temperature or the constant loading rate. Besides, they were restricted to uniaxial loading. The generalization of such models to multiaxial cases needs the consideration of equivalent forms of the stress and the strain or utilizing the critical plane theories [57]. Noting such difficulties, the energy-based models overcome these problems and even though, they consider both the stress and strain parameters in their formulations. Using such models facilitates the consideration of different loading conditions, the damage accumulation in samples and components with notches.

Therefore, a hysteresis energy-based model would be selected in this article in order to describe the fatigue lifetime of both AlSi and AlSi_N_T6 samples.

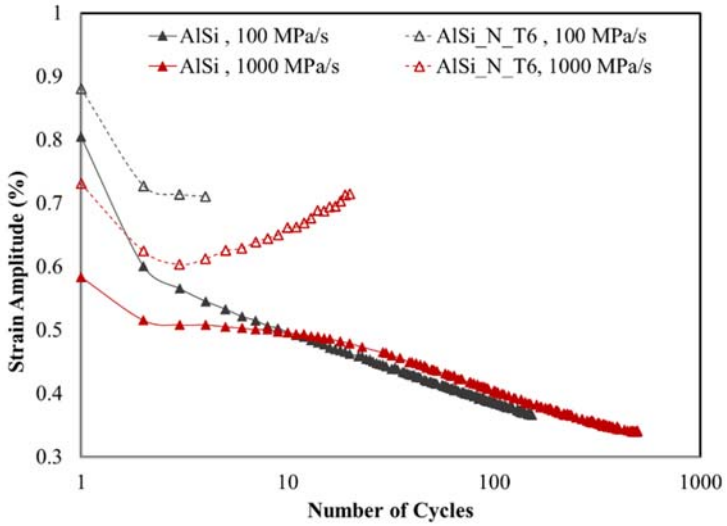

Figure 24: Test results regarding the stress rate effect under zero mean stress and the stress amplitude of 210 *MPa* for evolutions of the strain amplitude over cycles for both AlSi and AlSi_N_T6.

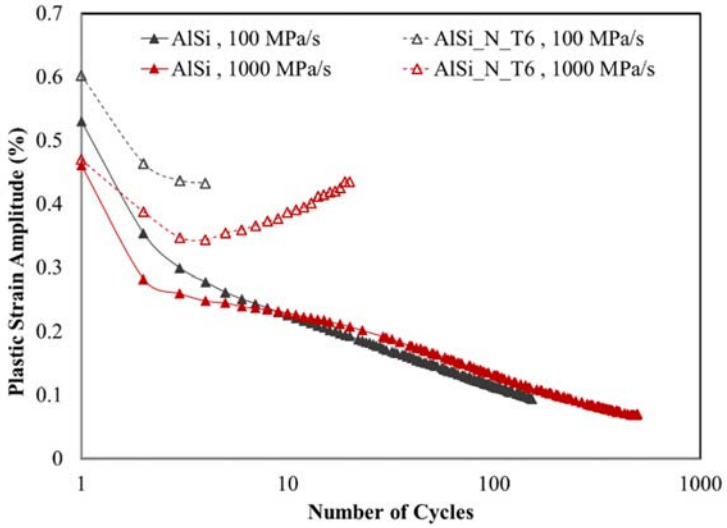

Figure 25: Test results regarding the stress rate effect under zero mean stress and the stress amplitude of 210 *MPa* for evolutions of the plastic strain amplitude over cycles for both AlSi and AlSi_N_T6.

The power-law formulation describing the relationship between the energy related damage parameter P and fatigue lifetime N_f has been described as follows [57]:

$$N_f = A(P)^{-B} \tag{1}$$

Where A and B are two material constants.
The energy related damage parameter that has been utilized in this investigation is the plastic strain energy density to represent the fatigue damage inside the material. The plastic strain energy at each cycle had been reported to be

representative of the necessary energy for the crack propagation [58]. Such a plastic strain energy is equal to the area of the stress-strain hysteresis loop, which could be written as follows [57]:

$$\Delta W_p = \oint \sigma d\varepsilon \approx \Delta\sigma\Delta\varepsilon_p \tag{2}$$

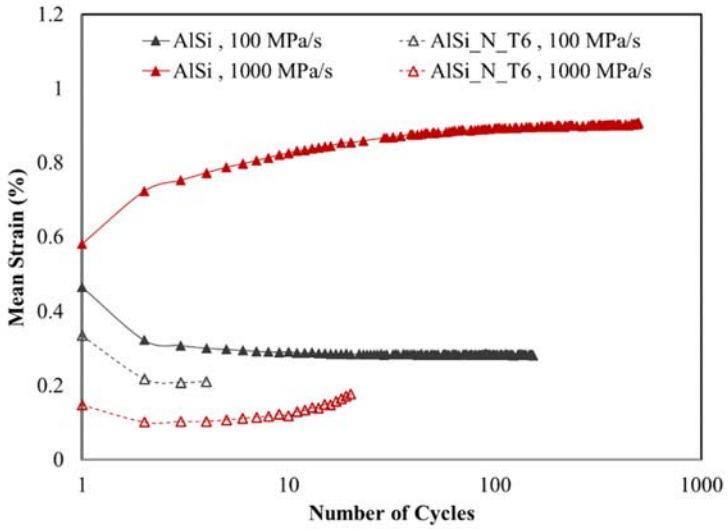

Figure 26: Test results regarding the stress rate effect under zero mean stress and the stress amplitude of 210 *MPa* for evolutions of the mean strain over cycles for both AlSi and AlSi_N_T6.

The literature [56] suggests that the plastic strain energy could be approximated as the product of the stress range, $\Delta\sigma$, and the plastic strain range, $\Delta\varepsilon_p$, determined at the mid-life hysteresis loop, instead of integrating the hysteresis area over cycles. It has been known primarily that the tensile mean stress has a detrimental effect on the fatigue lifetime [59-60], while the compressive mean stress has a beneficial effect. Therefore, the influence of mean stress has been embedded in lifetime prediction models as an additional parameter. It had been indicated in the "Cyclic behaviors" section that in some tests, the ratcheting phenomenon had been observed. Generally, the effect of ratcheting on the fatigue lifetime had been considered as the effect of the mean stress on the lifetime [61-62]. Therefore, in this investigation, the mean stress effect on the fatigue lifetime has been considered as an additional factor.
The plastic strain energy damage parameter has been modified to the following formulation [57]:

$$N_f = A\left(\Delta W_p\left[\left(1+m_1\frac{\sigma_m}{\sigma_a}\right)^{m_2}\right]\right)^{-B} \tag{3}$$

Where m_1 and m_2 are two material constants.
The value of material constants is calibrated using experimental data by a regression approach. The values of these parameters for both AlSi and AlSi_N_T6 had been reported in Tab. 6. Figs. 27-28 depictes the regression analysis on fatigue data of both AlSi and AlSi_N_T6 in a logarithmic scale analyzed by the plastic strain energy (PSE) model and its counterpart corrected version based on the mean stress effect. The coefficient of determination (CD) or the R^2 value has been considered for evaluating fitting capability of the lifetime model. The related formulation of the CD parameter has been presented in the literature [57]. As it could be observed, the coefficient of determination (CD) of AlSi_N_T6 data was smaller in value than AlSi data since the scatter in nano-composite data was larger. It is interesting to note that the mean stress correction factor in the energy model could enhance the accuracy of the model significantly, especially in the case of AlSi_N_T6. This argument could be proved by noting the CD parameter as its value increases in the PSE model with the addition of the mean stress effect. Besides, it has been proven that the dissipated plastic strain energy has a reverse relationship with the fatigue lifetime, which implied a negative slope in the following diagrams. Such a negative slope had not been seen for AlSi_N_T6 based on the uncorrected model but after the embedding of the mean stress correction factor into the models, the mentioned condition has been satisfied.

Material	Without correction		With mean stress correction			
	A	*B*	*A*	*B*	m_1	m_2
AlSi	9.8444	-0.4678	12.6252	-0.5016	2.0000	3.1000
AlSi_N_T6	2.4013	0.0522	3.6743	-0.2970	0.9900	-13.1000

Table 6: The martial constants of un-corrected and corrected plastic strain energy based on mean stress effect for both AlSi and AlSi_N_T6.

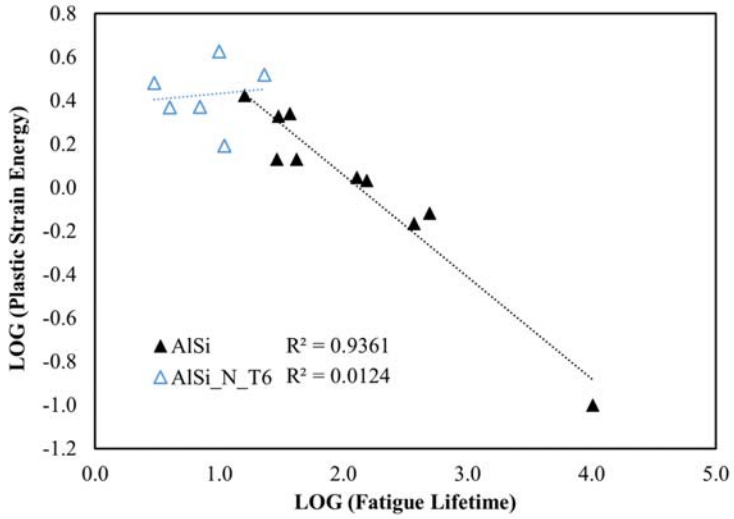

Figure 27: The regression analysis of the energy model for both AlSi alloys and AlSi_N_T6 without the mean stress correction factor.

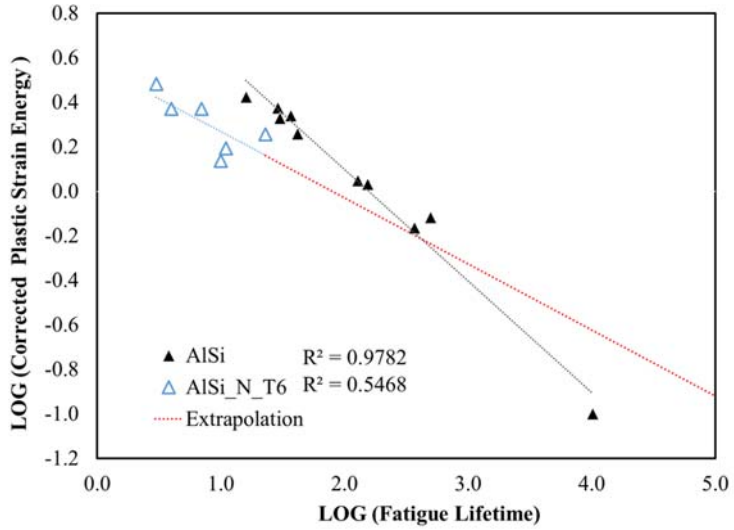

Figure 28: The regression analysis of the energy model for both AlSi alloys and AlSi_N_T6 with the mean stress correction factor.

By the extrapolation of the fitted curve for AlSi_N_T6, as a claim, it could be predicted that for lower stress/strain amplitudes, the fatigue lifetime for the heat-treated nano-composite specimens could be equal to or higher than that for non-heat-treatment samples.

Fig. 29 illustrates the scatter-band analysis for both AlSi alloys and AlSi_N_T6 with the consideration of uncorrected and corrected plastic strain energy models. It could be observed that the scatter-band for AlSi_N_T6 data had significantly wider than the data corresponding to AlSi alloys. Such results explained the higher value of CD for AlSi alloys in comparison to nano-composites. It was seen that the energy model with the correction factor presented a smaller scatter-band in both

cases of AlSi and AlSi_N_T6 samples in comparison to the un-corrected plastic strain energy model. It could be observed in Fig. 29 that the scatter-band parameter for AlSi alloys with the un-corrected model was about 2.5, while the corrected model presented the value of 1.6. Furthermore, in the case of AlSi_N_T6, the scatter-band in the uncorrected model was about 5000, while with the addition of the mean stress correction factor, the scatter-band parameter decreased considerably to about 3.

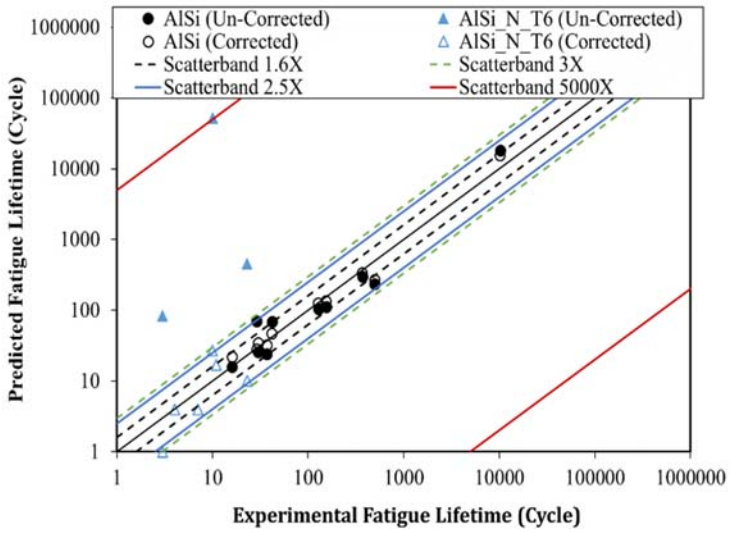

Figure 29: The scatter-band analysis of the fatigue data of both AlSi alloys and AlSi_N_T6.

It could be claimed that the present energy approach had a satisfying accuracy in the stress-controlled LCF lifetime prediction. The addition of a mean stress correction factor could enhance the accuracy of the model and also provide good results for the fatigue lifetime prediction in ratcheting-fatigue interaction cases. The simplicity and the consideration of both stress and strain parameters were other advantages of the presented model.
As it could be seen in Figs. 27-28, the addition of the reinforcement by nano-clay particles and the heat treatment influenced the fatigue lifetime significantly. In many samples, the fatigue lifetime decreased more than 50%. Such a result was in an agreement with the literature [9-11].

Discussion

The microstructure, tensile, and stress-controlled LCF behaviors of AlSi alloys and AlSi_N_T6 nano-composites have thoroughly described in previous sections. It had been shown that the piston aluminum alloy presented a weaker and softer behavior in both tensile and fatigue experiments after the nano-particles addition and the heat treatment. In the two following sections, the role of nano-particles and the heat treatment on such a behavior will be discussed.

Effect of nano-clay particles

Most of the studies [3-7,30-35,49-52] had proved that the nano-particles addition to the aluminum alloy results in an enhancement of mechanical properties. Such an enhancement had been attributed to several strengthening mechanisms including Hall-Petch strengthening, enhanced dislocation density, Orowan strengthening, and load transfer effect. As it had shown in Tab. 5, the results of the present investigation were in contradiction with mentioned studies. It has been reported in the literature [7,30] that beyond a threshold nano-particles volume/weight fraction, the strength and elongation of Aluminum Matrix Nano-composites (AMNCs) would be declined as a result of excessive presence of particle agglomerations and micro-porosities. Also, very high casting temperature, stirring velocity, and time had been reported [30] to produce degraded mechanical properties in the stir-casting process. Since the elongation of AlSi_N_T6 in the present investigation has increased after the nano-particles addition and the heat treatment, the nano-particles cannot be considered as the major source of the poor performance of AlSi_N_T6. Particle agglomerations and micro-porosities would decrease the yield and ultimate tensile strengths as well as ductility of the material because of providing potential sites for crack initiation and accelerating the crack propagation.
It has been indicated in Figs. 9-10 that some degrees of agglomerations are present in AlSi_N_T6. Nevertheless, with a qualitative comparison with similar micrographs of AMMNCs [6,7,30,51] the dispersion of nano-particles demonstrated no

intensive heterogeneity and there were no large agglomerations (larger than 1 micrometer) exist in the microstructure of AlSi_N_T6.
The higher porosity content in AlSi_N_T6 in comparison to the AlSi alloy had been reported in Tab. 4. It had been shown [63] that the aluminum alloy with 10 *wt.*% nano-clay particles corresponding to 3.60% porosity content still offered enhanced strength and decreased ductility in comparison to the monolithic alloy. Particle agglomerations and micro-porosities were characteristic features of nano-composites. Their formation was inevitable during the processing of such materials; however, it was reported that nano-composites processed by the compo-casting method [49], the ultrasonic cavitation [46], and the extrusion after casting [50] offered lower agglomerations and porosities content in comparison to the stir-casting method.
It had been observed in Figs. 23-26 that AlSi_N_T6 produced a cyclic softening behavior with more plastic strain amplitudes regarding the AlSi monolithic alloy. It had been proved in the literature [8-12,27,28] that the dislocation hindering role of ceramic particles results in a higher rate of cyclic hardening response and also the lower exhibited plastic strain. The response of nano-composites is the same but more effective in that way because of more particulate content in comparison to micro-particles with the same volume fraction. The results of the present investigation also disagree with the mentioned phenomena. Such a poor fatigue performance of AlSi_N_T6 also follows the tensile properties. In general, it could be claimed that particle agglomerations and micro-porosities were not able to increase the ductility alongside the material strength reduction. The nano particles affected the response of AlSi_N_T6 but it could be claimed that the major source of poor performance of AlSi_N_T6 was the heat treatment.

Effect of heat treatment

The studies on AMNCs have accounted for the T6 heat treatment as an improver of mechanical properties [7,51,63-66] and also the fatigue properties [51,67-69] but such a positive effect has not been observed in the results of the present investigation. It could be claimed that the poor performance of AlSi_N_T6 was related to the excessive aging time and temperature of the T6 process. As it had been indicated in Figs. 2-5, the size and the circularity of Si particles within the microstructure of AlSi alloys enhanced after the nano-particles addition and the heat treatment. The spheroidization and the size reduction of eutectic Si particles have been reported to be the results of the solution treatment and artificial aging, respectively during T6 heat treatment [67]. Besides, the nano-particles addition had some effects on the size reduction of the eutectic Si as a result of enhanced Si particles nucleation at the nano-particles site. Such a change in the morphology could explain the significant strengthening and the increase in the ductility [51,66]; however, the reduction in the size of Si particles had not been met in this research. This observation implied a T7 over-aged state of AlSi_N_T6.
It has been reported in several studies [51,68] that the presence of the nano-reinforcement could change the aging kinetics of the material. The segregation of elements like Mg at the matrix-reinforcement interface and grain boundaries, which resulted in the prevention of forming Mg_2Si or $MgZn_2$ precipitates, had been reported to reduce the precipitation hardening and subsequently, the detrition of mechanical properties.
Regarding the above statements, it is necessary to use the lower aging time and temperature in comparison to those normally used in the literature for nano-composite materials [65] and inevitably optimize the heat treatment parameters with the objective of reaching the optimum strength and ductility combination in aluminum-based nano-composites. Such a work could be reserved for the future work.
The weaker and softer behavior of AlSi_N_T6 during tensile tests could explain the cyclic softening behavior under stress-controlled LCF loading. As it was reported in the literature [67], the excess aging time or temperature during T6 heat treatment could result in cyclic softening of the A356 alloy and subsequently producing severe plastic deformation in the material. Therefore, the wrongly chosen aging time and temperatures for AlSi_N_T6 appeared as the lower resistance of AlSi_N_T6 against the applied cyclic stress. It was obvious in Fig. 26 that the reduced ability of AlSi_N_T6 to the tensile deformation noting on the compressive mean strain in AlSi_N_T6 nano-composites even though the applied mean stress was zero. Therefore, AlSi_N_T6 accommodated the deformation mostly by the compressive deformation. Such an anisotropy in tension and compression conditions could explain the ratcheting deformation in AlSi_N_T6, as could be observed in Fig. 18.

CONCLUSIONS

In this research, tensile and stress-controlled LCF properties of piston AlSi alloys, with and without heat treatment besides nano-clay particles was investigated. The obtained experimental data showed the following highlights and behaviors:

- The heat treatment could increase the size and circularity of the silicon phases.

- Some small degrees of agglomerated nano-particles are detected in the microstructure.
- The porosity content of AlSi alloy was enhanced after the nano-particles addition.
- The mechanical properties of the AlSi alloy decreased after the nano-particles addition and the hat-treatment.
- The cyclic response of the AlSi alloy after the nano-particles addition and the heat treatment changed from a cyclic hardening feature to a cyclic softening feature.
- The resistance of the AlSi alloy against the ratcheting deformation reduces after the nano-particles addition and the heat treatment. The ratcheting deformation was observed in some nano-composite samples, even at zero mean stress.
- A tensile mean strain is observed in many tests at fully-reversed stress cycling. Such a result implied the decreased resistance of the material against the tensile deformation, especially for nano-composite.
- Nano-composite presented a rate-dependent response even at room temperature, unlike its counterpart monolithic alloy.
- The fatigue lifetime of nano-composite was mostly less than 50% in comparison to its counterpart monolithic alloy.
- It was shown that the major source of mechanical and fatigue properties degradation of nano-composite was related to the excessive aging time as a result of neglecting the higher aging kinetics in nano-composite.
- The fatigue lifetime prediction of samples was done using a plastic strain energy approach. It was shown that the addition of a mean stress correction factor to the model could enhance the accuracy of the model considerably.

For the further investigation, the fracture surface analysis could be performed on the failed sample (after the tests), in order to find the failure mechanism and the fracture behavior of the material. Moreover, this report could be considered to find the influence of the nano-clay addition and the heat treatment on the fracture behavior and the failure mechanism of studied materials, besides the effect of the mean stress, the stress amplitude and the stress rate. Moreover, performing a higher number of LCF testing on nano-composite samples with a pre-designed plan for loading conditions could help the researcher to investigate the material behavior in a high accurate state.

ACKNOWLEDGEMENT

Through the IMPULSE Program, this project was financed by the Austrian Agency for International Cooperation in Education and Research (OeAD) and the Ministry of Science, Research and Technology of the Islamic Republic of Iran and also Kharazmi University. Moreover, authors thank the MPN company in Iran for providing the initial aluminum ingots.

REFERENCES

[1] Silva, F.S. (2006). Fatigue on engine pistons - A compendium of case studies, Eng. Fail. Anal., 13(3), pp. 480–492, DOI: 10.1016/j.engfailanal.2004.12.023.

[2] Azadi, M. (2013). Effects of strain rate and mean strain on cyclic behavior of aluminum alloys under isothermal and thermo-mechanical fatigue loadings, Int. J. Fatigue, 47, pp. 148–153, DOI: 10.1016/j.ijfatigue.2012.08.005.

[3] Prasad Reddy, A., Vamsi Krishna, P., Narasimha Rao, R., Murthy, N. V. (2017). Silicon Carbide Reinforced Aluminium Metal Matrix Nano Composites-A Review. Materials Today: Proceedings, 4(2), pp. 3959–3971, DOI: 10.1016/j.matpr.2017.02.296.

[4] Bhoi, N.K., Singh, H., Pratap, S. (2020). Developments in the aluminum metal matrix composites reinforced by micro/nano particles – A review, J. Compos. Mater., 54(6), pp. 813–833, DOI: 10.1177/0021998319865307.

[5] Tahamtan, S., Halvaee, A., Emamy, M., Zabihi, M.S. (2013). Fabrication of Al/A206-Al2O3 nano/micro composite by combining ball milling and stir casting technology, Mater. Des., 49, pp. 347–359, DOI: 10.1016/j.matdes.2013.01.032.

[6] Sajjadi, S.A., Torabi Parizi, M., Ezatpour, H.R., Sedghi, A. (2012). Fabrication of A356 composite reinforced with micro and nano Al 2O3 particles by a developed compocasting method and study of its properties, J. Alloys Compd., 511(1), pp. 226–231, DOI: 10.1016/j.jallcom.2011.08.105.

[7] Karbalaei Akbari, M., Baharvandi, H.R., Shirvanimoghaddam, K. (2015). Tensile and fracture behavior of nano/micro TiB2 particle reinforced casting A356 aluminum alloy composites, Mater. Des., 66, pp. 150–161, DOI: 10.1016/j.matdes.2014.10.048.

[8] Luk, M.J., Mirza, F.A., Chen, D.L., Ni, D.R., Xiao, B.L., Ma, Z.Y. (2015). Low cycle fatigue of SiCp reinforced AA2009 composites, Mater. Des., 66, pp. 274–283, DOI: 10.1016/j.matdes.2014.10.070.
[9] Koh, S.K., Oh, S.J., Li, C., Ellyin, F. (1999). Low-cycle fatigue life of SiC-particulate-reinforced Al-Si cast alloy composites with tensile mean strain effects, Int. J. Fatigue, 21(10), pp. 1019–1032, DOI: 10.1016/S0142-1123(99)00099-7.
[10] Han, N.L., Wang, Z.G., Lizhi Sun, (1995). Effect of reinforcement size on low cycle fatigue behavior of SiC particle reinforced aluminum matrix composites, Scr. Metall. Mater., 33(5), pp. 781–787, DOI: 10.1016/0956-716X(95)00281-Y.
[11] Srivatsan, T.S. (1995). Cyclic strain resistance and fracture behaviour of Al2O3-particulate-reinforced 2014 aluminium alloy metal-matrix composites, Int. J. Fatigue, 17(3), pp. 183–199, DOI: 10.1016/0142-1123(95)98939-Z.
[12] Gasem, Z.M., Ali, S.S. (2013). Low-cycle fatigue behavior of powder metallurgy 6061 aluminum alloy reinforced with submicron-scale Al2O3 particles, Mater. Sci. Eng. A, 562, pp. 109–117, DOI: 10.1016/j.msea.2012.10.097.
[13] LLorca, J. (2002). Fatigue of particle-and whisker-reinforced metal-matrix composites, Prog. Mater. Sci., 47(3), pp. 283–353, DOI: 10.1016/S0079-6425(00)00006-2.
[14] Wallin, K., Saario, T., Törrönen, K. (1986). Fracture of brittle particles in a ductile matrix, Int. J. Fracture, 32, pp. 201-209, DOI: 10.1007/BF00018353.
[15] Senthilkumar, R., Arunkumar, N., Manzoor Hussian, M. (2015). A comparative study on low cycle fatigue behaviour of nano and micro Al2O3 reinforced AA2014 particulate hybrid composites, Results Phys., 5, pp. 273–280, DOI: 10.1016/j.rinp.2015.09.004.
[16] Azadi, M., Bahmanabadi, H., Gruen, F., Winter, G. (2020). Evaluation of tensile and low-cycle fatigue properties at elevated temperatures in piston aluminum-silicon alloys with and without nano-clay-particles and heat treatment, Mater. Sci. Eng. A, 788, 139497, DOI: 10.1016/j.msea.2020.139497.
[17] Ghasemi Yazdabadi, H., Ekrami, A., Kim, H.S., Simchi, A. (2013). An investigation on the fatigue fracture of P/M Al-SiC nanocomposites, Metall. Mater. Trans. A Phys. Metall. Mater. Sci., 44, pp. 2662–2671, DOI: 10.1007/s11661-013-1620-3.
[18] Jabbari, A.H., Shafiee Sabet, A., Sedighi, M., Jahed, H., Sommitsch, C. (2020). Low cycle fatigue behavior of magnesium matrix nanocomposite at ambient and elevated temperatures, Mater. Sci. Eng. A, 793, pp. 139890, DOI: 10.1016/j.msea.2020.139890.
[19] Zhang, B., Wang, R., Hu, D., Jiang, K., Mao, J., Jing, F., Hao, X. (2021). Stress-controlled LCF experiments and ratcheting behaviour simulation of a nickel-based single crystal superalloy with [001] orientation, Chinese J. Aeronaut., 34(8), pp. 112–121, DOI: 10.1016/j.cja.2020.05.030.
[20] Chang, L., Zhou, B. Bin., Ma, T.H., Li, J., He, X.H., Zhou, C.Y. (2019). Comparisons of low cycle fatigue behavior of CP-Ti under stress and strain-controlled modes in transverse direction, Mater. Sci. Eng. A, 746, pp. 27–40, DOI: 10.1016/j.msea.2018.12.125.
[21] Agius, D., Wallbrink, C., Kourousis, K.I. (2017). Cyclic elastoplastic performance of aluminum 7075-T6 under strain- and stress-controlled loading, J. Mater. Eng. Perform., 26, pp. 5769–5780, DOI: 10.1007/s11665-017-3047-2.
[22] Sreenivasan, S., Mishra, S.K., Dutta, K. (2017). Ratcheting strain and its effect on low cycle fatigue behavior of Al 7075-T6 alloy, Mater. Sci. Eng. A, 698, pp. 46–53, DOI: 10.1016/j.msea.2017.05.048.
[23] Dutta, K., Ray, K.K. (2012). Ratcheting phenomenon and post-ratcheting tensile behaviour of an aluminum alloy, Mater. Sci. Eng. A, 540, pp. 30–37, DOI: 10.1016/j.msea.2012.01.024.
[24] Kreethi, R., Verma, P., Dutta, K. (2015). Influence of heat treatment on ratcheting fatigue behavior and post ratcheting tensile properties of commercial aluminum, Trans. Indian Inst. Met., 68, pp. 229–237, DOI: 10.1007/s12666-014-0449-9.
[25] Wang, Y., Yang, S., Xie, C., Liu, H., Zhang, Q. (2018). Microstructure and ratcheting behavior of additive manufactured 4043 aluminum alloy, J. Mater. Eng. Perform., 27, pp. 4582–4592, DOI: 10.1007/s11665-018-3563-8.
[26] Mishra, S.K., Roy, H., Mondal, A.K., Dutta, K. (2017). Damage assessment of A356 Al alloy under ratcheting-creep interaction, Metall. Mater. Trans. A Phys. Metall. Mater. Sci., 48, pp. 2877–2885, DOI: 10.1007/s11661-017-4077-y.
[27] Kang, G. (2006). Uniaxial time-dependent ratchetting of SiCP/6061Al composites at room and high temperature, Compos. Sci. Technol., 66(10), pp. 1418–1430, DOI: 10.1016/j.compscitech.2005.09.002.
[28] Kang, G.Z., Liu, Y.J. (2007). Uniaxial and multiaxial cyclic deformation behaviors of SiCp/6061Al alloy composites, Key Eng. Mater., 353-358, pp. 1247–1250, DOI: 10.4028/www.scientific.net/kem.353-358.1247.
[29] Goh, C.S., Gupta, M., Wei, J., Lee, L.C. (2008). The cyclic deformation behavior of Mg-Y2O3 nanocomposites, J. Compos. Mater., 42(19), pp. 2039–2050, DOI: 10.1177/0021998308094544.

[30] Dehghan Hamedan, A., Shahmiri, M. (2012). Production of A356-1wt% SiC nanocomposite by the modified stir casting method, Mater. Sci. Eng. A, 556, pp. 921–926, DOI: 10.1016/j.msea.2012.07.093.
[31] Juang, S.H., Fan, L.J., Yang, H.P.O. (2015). Influence of preheating temperatures and adding rates on distributions of fly ash in aluminum matrix composites prepared by stir casting, Int. J. Precis. Eng. Manuf., 16, pp. 1321–1327, DOI: 10.1007/s12541-015-0173-3.
[32] Azadi, M., Zolfaghari, M., Rezanezhad, S., Azadi, M. (2018). Effects of SiO2 nano-particles on tribological and mechanical properties of aluminum matrix composites by different dispersion methods, Appl. Phys. A Mater. Sci. Process., 124, pp. 1–13, DOI: 10.1007/s00339-018-1797-9.
[33] Karbalaei Akbari, M., Mirzaee, O., Baharvandi, H.R. (2013). Fabrication and study on mechanical properties and fracture behavior of nanometric Al2O3 particle-reinforced A356 composites focusing on the parameters of vortex method, Mater. Des., 46, pp. 199–205, DOI: 10.1016/j.matdes.2012.10.008.
[34] Zeren, M. (2007). The effect of heat-treatment on aluminum-based piston alloys, Mater. Des., 28(9), pp. 2511–2517, DOI: 10.1016/j.matdes.2006.09.010.
[35] Nassar, A.E., Nassar, E.E. (2017). Properties of aluminum matrix nano composites prepared by powder metallurgy processing, J. King Saud Univ. - Eng. Sci., 29(3), pp. 295–299, DOI: 10.1016/j.jksues.2015.11.001.
[36] ASTM E8 / E8M-11, (2011). Standard Test Methods for Tension Testing of Metallic Materials, ASTM Int. West Conshohocken, PA, , DOI: 10.1520/E0008_E0008M-13A.
[37] ASTM E466 - 15, (2015). Standard Practice for Conducting Force Controlled Constant Amplitude Axial Fatigue Tests of Metallic Materials. DOI: 10.1520/E0466-15.
[38] Casati, R., Vedani, M. (2014). Metal Matrix Composites Reinforced by Nano-Particles – A Review, Metals (Basel)., 4(1), pp. 65–83, DOI: 10.3390/met4010065.
[39] Zainon, F., Rafezi Ahmad, K., Daud, R. (2015). Effect of heat treatment on microstructure, hardness and wear of aluminum alloy 332, Appl. Mech. Mater., 786, pp. 18–22, DOI: 10.4028/www.scientific.net/amm.786.18.
[40] Shi, W., Gao, B., Tu, G., Li, S., Hao, Y., Yu, F. (2010). Effect of neodymium on primary silicon and mechanical properties of hypereutectic Al-15Si alloy, J. Rare Earths, 28(SUPPL. 1), pp. 367–370, DOI: 10.1016/S1002-0721(10)60363-8.
[41] Chen, C., Liu, Z. xia., Ren, B., Wang, M. xing., Wang, Y. gang., Liu, Z. yong. (2007). Influences of complex modification of P and RE on microstructure and mechanical properties of hypereutectic Al-20Si alloy, Trans. Nonferrous Met. Soc. China (English Ed., 17(2), pp. 301–306, DOI: 10.1016/S1003-6326(07)60089-2.
[42] Zhu, M., Jian, Z., Yang, G., Zhou, Y. (2012). Effects of T6 heat treatment on the microstructure, tensile properties, and fracture behavior of the modified A356 alloys, Mater. Des., 36, pp. 243–249, DOI: 10.1016/j.matdes.2011.11.018.
[43] Pio, L.Y. (2011). Effect of T6 heat treatment on the mechanical properties of gravity die cast A356 aluminium alloy, J. Appl. Sci., 11(11), pp. 2048–2052, DOI: 10.3923/jas.2011.2048.2052.
[44] Rezanezhad, S., Azadi, M., Azadi, M. (2021). Influence of heat treatment on high-cycle fatigue and fracture behaviors of piston aluminum alloy under fully-reversed cyclic bending, Met. Mater. Int., 27, pp. 860–870, DOI: 10.1007/s12540-019-00498-7.
[45] Zolfaghari, M., Azadi, M., Azadi, M. (2021). Characterization of high-cycle bending fatigue behaviors for piston aluminum matrix SiO2 nano-composites in comparison with aluminum-silicon alloys, Int. J. Met., 15, pp. 152–168, DOI: 10.1007/s40962-020-00437-y.
[46] Salehi, A., Babakhani, A., Zebarjad, S.M. (2015). Microstructural and mechanical properties of Al-SiO2 nanocomposite foams produced by an ultrasonic technique, Mater. Sci. Eng. A, 638, pp. 54–59, DOI: 10.1016/j.msea.2015.04.024.
[47] Han, L., Sui, Y., Wang, Q., Wang, K., Jiang, Y. (2017). Effects of Nd on microstructure and mechanical properties of cast Al-Si-Cu-Ni-Mg piston alloys, J. Alloys Compd., 695, pp. 1566–1572, DOI: 10.1016/j.jallcom.2016.10.300.
[48] Firouzdor, V., Rajabi, M., Nejati, E., Khomamizadeh, F. (2007). Effect of microstructural constituents on the thermal fatigue life of A319 aluminum alloy, Mater. Sci. Eng. A, 454–455, pp. 528–535, DOI: 10.1016/j.msea.2007.01.018.
[49] Sajjadi, S.A., Ezatpour, H.R., Torabi Parizi, M. (2012). Comparison of microstructure and mechanical properties of A356 aluminum alloy/Al2O3 composites fabricated by stir and compo-casting processes, Mater. Des., 34, pp. 106–111, DOI: 10.1016/j.matdes.2011.07.037.
[50] Ezatpour, H.R., Sajjadi, S.A., Sabzevar, M.H., Huang, Y. (2014). Investigation of microstructure and mechanical properties of Al6061-nanocomposite fabricated by stir casting, Mater. Des., 55, pp. 921–928, DOI: 10.1016/j.matdes.2013.10.060.
[51] Ahmed, A., Neely, A.J., Shankar, K., Nolan, P., Moricca, S., Eddowes, T. (2010). Synthesis, tensile testing, and microstructural characterization of nanometric sic particulate-reinforced Al 7075 matrix composites, Metall. Mater. Trans. A Phys. Metall. Mater. Sci., 41, pp. 1582–1591, DOI: 10.1007/s11661-010-0201-y.

[52] Choi, H., Jones, M., Konishi, H., Li, X. (2012). Effect of combined addition of Cu and aluminum oxide nanoparticles on mechanical properties and microstructure of Al-7Si-0.3Mg alloy, Metall. Mater. Trans. A Phys. Metall. Mater. Sci., 43, pp. 738–746, DOI: 10.1007/s11661-011-0905-7.
[53] Akbari, M.K., Baharvandi, H.R., Mirzaee, O. (2013). Nano-sized aluminum oxide reinforced commercial casting A356 alloy matrix: Evaluation of hardness, wear resistance and compressive strength focusing on particle distribution in aluminum matrix, Compos. Part B Eng., 52, pp. 262–268, DOI: 10.1016/j.compositesb.2013.04.038.
[54] Kwofie, S., Chandler, H.D. (2007). Fatigue life prediction under conditions where cyclic creep-fatigue interaction occurs, Int. J. Fatigue, 29(12), pp. 2117–2124, DOI: 10.1016/j.ijfatigue.2007.01.022.
[55] Basquin, O. H. (1910). The Exponential Law of Endurance Tests, Am. Soc. Test. Mater. Proc., 10, pp. 625–30.
[56] Kwofie, S., Chandler, H.D. (2001). Low cycle fatigue under tensile mean stresses where cyclic life extension occurs, Int. J. Fatigue, 23(4), pp. 341–345, DOI: 10.1016/S0142-1123(00)00098-0.
[57] Farrahi, G.H., Azadi, M., Winter, G., Eichlseder, W. (2013). A new energy-based isothermal and thermo-mechanical fatigue lifetime prediction model for aluminium-silicon-magnesium alloy, Fatigue Fract. Eng. Mater. Struct., 36(12), pp. 1323–1335, DOI: 10.1111/ffe.12078.
[58] Skelton, R.P. (1991). Energy criterion for high temperature low cycle fatigue failure, Mater. Sci. Technol., 7(5), pp. 427–440, DOI: 10.1179/mst.1991.7.5.427.
[59] Ostergren, W. (1976). A damage function and associated failure equations for predicting hold time and frequency effects in elevated temperature, low cycle fatigue, J. Test. Eval., 4(5), 339, DOI: 10.1520/JTE10520J.
[60] Pawliczek, R., Rozumek, D. (2020). Cyclic tests of smooth and notched specimens subjected to bending and torsion taking into account the effect of mean stres, Mater., 13(9), 2141, DOI: 10.3390/ma13092141.
[61] Rozumek, D., Faszynka, S., (2017). Fatigue crack growth in 2017A-T4 alloy subjected to proportional bending with torsion, Frattura ed Integrità Strutturale, 11(42), pp. 23–29, DOI: 10.3221/IGF-ESIS.42.03.
[62] Kreethi, R., Sivateja, C., Mondal, A.K., Dutta, K. (2019). Ratcheting life prediction of quenched-tempered 42CrMo4 steel, J. Mater. Sci., 54, pp. 11703–11712, DOI: 10.1007/s10853-019-03705-3.
[63] Pan, X.M., Li, X., Chang, L., Zhang, G.D., Xue, F., Zhao, Y.F., Zhou, C.Y. (2018). Thermal-mechanical fatigue behavior and lifetime prediction of P92 steel with different phase angles, Int. J. Fatigue, 109, pp. 126–136, DOI: 10.1016/j.ijfatigue.2017.12.021.
[64] Gholipour, V., Shamanian, M., Ashrafi, A., Maleki, A. (2020). Development of aluminium-nanoclay composite by using powder metallurgy and hot extrusion process, Met. Mater. Int., , pp. 1–14, DOI: 10.1007/s12540-020-00791-w.
[65] Knowles, A.J., Jiang, X., Galano, M., Audebert, F. (2015). Microstructure and mechanical properties of 6061 Al alloy based composites with SiC nanoparticles, J. Alloys Compd., 615(Supplement 1), pp. S401–S405, DOI: 10.1016/j.jallcom.2014.01.134.
[66] El-Mahallawi, I., Abdelkader, H., Yousef, L., Amer, A., Mayer, J., Schwedt, A. (2012). Influence of Al2O3 nano-dispersions on microstructure features and mechanical properties of cast and T6 heat-treated Al Si hypoeutectic Alloys, Mater. Sci. Eng. A, 556, pp. 76–87, DOI: 10.1016/j.msea.2012.06.061.
[67] Azadi, M., Shirazabad, M.M. (2013). Heat treatment effect on thermo-mechanical fatigue and low cycle fatigue behaviors of A356.0 aluminum alloy, Mater. Des., 45, pp. 279–285, DOI: 10.1016/j.matdes.2012.08.066.
[68] Shaha, S.K., Czerwinski, F., Kasprzak, W., Friedman, J., Chen, D.L. (2016). Effect of Mn and heat treatment on improvements in static strength and low-cycle fatigue life of an Al-Si-Cu-Mg alloy, Mater. Sci. Eng. A, 657, pp. 441–452, DOI: 10.1016/j.msea.2016.01.015.
[69] Borrego, L.P., Abreu, L.M., Costa, J.M., Ferreira, J.M. (2004). Analysis of low cycle fatigue in AlMgSi aluminium alloys, Eng. Fail. Anal., 11(5), pp. 715–725, DOI: 10.1016/j.engfailanal.2003.09.003.